BOREAL ENVIRONMENT RESEARCH 21: 332–344
ISSN 1239-6095 (print) ISSN 1797-2469 (online)

Helsinki 23 May 2016

Seasonal variation and characterisation of reactive trace gas mixing ratios over a hemi-boreal mixed forest site in Estonia

Steffen M. Noe[1)]*, Dmitrii Krasnov[1)], Alisa Krasnova[1)], H. Peter E. Cordey[1)] and Ülo Niinemets[1)2)]

[1)] *Estonian University of Life Sciences, Institute of Agricultural and Environmental Sciences, Department of Plant Physiology, Kreutzwaldi 1, EE-51014 Tartu, Estonia (*corresponding author's e-mail: steffen.noe@emu.ee)*
[2)] *Estonian Academy of Sciences, Kohtu 6, EE-10130 Tallinn, Estonia*

Received 8 Sep. 2015, final version received 13 Jan. 2016, accepted 14 Jan. 2016

Noe S.M., Krasnov D., Krasnova A., Cordey H.P.E. & Niinemets Ü. 2016: Seasonal variation and characterisation of reactive trace gas mixing ratios over a hemi-boreal mixed forest site in Estonia. *Boreal Env. Res.* 21: 332–344.

Tropospheric mixing ratios of reactive trace gases (ozone, sulphur dioxide, nitric oxide and nitrogen dioxide) together with meteorological parameters were measured at SMEAR Estonia (Järvselja, Estonia) from August 2013 until May 2015. Seasonal monthly median mixing ratios of the trace gases were determined. Data of incoming wind directions were used to divide the site into four quadrants to compare the median mixing ratios among quadrants. We calculated 48-hour back-trajectories from January to May 2015 for days with different trace gas mixing ratios to determine the influence of pollutant transport and the impact of local processes on ambient mixing ratios. Overall, long-distance transport contributed to 15% of the total concentrations measured. The data demonstrate that distant air masses carrying higher pollutant concentrations, in particular from eastern directions, significantly contributed to local SO_2 and NO_x mixing ratios. Otherwise, the SMEAR Estonia station is a rural site with pollutant mixing ratios near to the measurement equipment's detection limit.

Introduction

Reactive trace gases play an important role in the formation and growth of atmospheric aerosols. Recent research shows their participation in the reactions related to the critical cluster stabilisation process leading to nucleation, and further in the reactions related to the cluster growth (Kerminen *et al*. 2012, Kulmala *et al*. 2013, Westervelt *et al*. 2014). New particle formation begins by forming clusters of molecules or ions. These need to be stabilised for the subsequent processes of condensation and coagulation growth (Kulmala *et al*. 2000a, Kulmala 2004). Inorganic trace gases like ozone (O_3), nitrogen oxides (NO_x) and sulphuric dioxide (SO_2) participate, as precursors to aerosols via photochemical reactions, in the formation of sulphuric acid (H_2SO_4), while NO_x further participates in O_3 formation, and they all collectively contribute to the oxidative state of the atmosphere (Kulmala *et al*. 2008, Karl *et al*. 2010, Foken *et al*. 2012). Especially over forests, reactions of O_3, NO and NO_2 with short-lived biogenic volatile organics (VOC) result in the formation of ELVOC (extreme low volatile organic compounds) which participate in the nucleation and secondary organic aerosol (SOA) formation processes (Hakola *et al*. 2003,

Editor in charge of this article: Veli-Matti Kerminen

Hewitt *et al*. 2011, Holopainen 2011, Rollins *et al*. 2012, Ehn *et al*. 2014, Jokinen *et al*. 2015). Aerosols can be formed and grown in size from naturally released organic precursors over boreal forests. These aerosols have been reported to affect clouds and, thereby, the radiative forcing and climate of boreal forests (Tunved *et al*. 2006, Kulmala *et al*. 2008, Spracklen *et al*. 2008).

Estonia is mainly covered by hemi-boreal mixed forests that have been reported to emit higher amounts of VOCs than boreal forest ecosystems located further north (Noe *et al*. 2011, 2012, Bourtsoukidis *et al*. 2014). Recent model estimates projected an increase in the area and movement towards north for this forest ecosystem under warmer future climate scenarios (Hickler *et al*. 2012). It has been pointed out that combining physical, chemical and biological knowledge together with state-of-the-art equipment providing continuous measurements of environmental and biological characteristics are needed to reduce uncertainties in explaining the direct and indirect aerosol effects on climate (Kulmala *et al*. 2000b, Hari and Kulmala 2005). Reactive trace gas mixing ratios at a given location are affected by both anthropogenic and biogenic sources (Kulmala *et al*. 2000b, Lyubovtseva *et al*. 2005, Foken *et al*. 2012). A tool for comprehensive observation of such integrated effects is the SMEAR station (Station for Measuring forest Ecosystem–Atmosphere Relations) (Hari and Kulmala 2005). In the summer 2013, the Estonian station (SMEAR Estonia) became operational, which allowed us to gather measurements of reactive trace gas mixing ratios from October 2013 until May 2015, assess their seasonal trends and determine whether local or distant sources alter the measured background mixing ratios. Such measurements are essential for studying the predictability of local trace gas background concentrations and aerosol formation events. Thus, they contribute to the development of applied models of aerosol and cloud formation and climate prediction.

The aims of this work were to characterise the seasonal changes of measured trace gases at the SMEAR Estonia station based on continuous measurements, to provide the first estimate of the contribution of local and distant pollution sources at the site, and to locate source regions according to chosen cases of increased and low-polluted episodes.

Experiments

The SMEAR Estonia station

The SMEAR Estonia station (58.2714°N, 27.2703°E, 36 m a.s.l.) is situated in a mixed, hemi-boreal forest stand comprising Scots pine (*Pinus sylvestris*), Norway spruce (*Picea abies*), silver birch (*Betula pendula*) and downy birch (*Betula pubescens*). The dominant tree species around the 130-m-high atmospheric measurement mast is Scots pine, constituting the top canopy, while Norway spruce and birch species form the sub-canopy layer (partly suppressed, partly growing into the upper canopy). The stand age in the surroundings of the measurement station varies due to the past forest management practices and reaches an age of more than 100 years. The mean canopy height at the measurement mast is 20 m, but within a distance of about 300 m the oldest stands can reach up to 30 m. The mean annual temperature in the area varies between 4 and 6 °C, the annual precipitation is 500–750 mm with about 40–80 mm as snow, and the growing season length is about 170–180 days. The location qualifies as rural background monitoring site (Noe *et al*. 2011).

The Järvselja village and Experimental Forestry Centre are located 1.2 km SSE of the SMEAR Estonia station and are inhabited by approximately 40 people. The village together with the road network consisting of primarily gravel roads is the only local pollution source that can occasionally affect the measurement site. A circular area within a radius of 2 km around the atmospheric mast was considered local source area, and everything beyond a distant source.

The cities nearest to the site are Tartu (about 100 000 inhabitants, 36 km NW) and Pskov (about 205 000 inhabitants, 79 km SE across lake Peipus), but both are located outside the major wind direction coming towards the station. Within a distance of approximately 10 km N of SMEAR Estonia, the Peipsiveere Nature Reserve (346 km^2) is situated, while

Lake Peipsi (3555 km^2) is located NE of the station. The distance to the lake is 8 km to the east and 11 km to the north.

Measurements

Continuous measurements of O_3, NO_x and SO_2 concentrations started in autumn 2013 at the ground level (2 m) outside the forest and lasted for about one year at that height. The concentration of NO_x was calculated as the sum of NO and NO_2. In October 2014, the sample system was connected to the mast and the measurement height increased to 30 m. The ambient air was drawn through PTFE tubes from the site of the measurement to the main cottage by a side channel blower pump (Busch SB 0800, Busch Produktions GmbH, Maulburg, Germany), ensuring turbulent flow inside the tube. From the main air stream, a portion was drawn to the analysers by a second pump (KNF N87TTE, KNF Neuberger GmbH, Freiburg, Germany). That diverted flow was slightly higher than the summed flow needed by the analysers and the excess was exhausted via a T-piece allowing to measure at the atmospheric pressure. The tube system was covered to protect against direct sunlight and heated to avoid condensation.

The O_3 concentration was measured with a Thermo (Model 49i) analyser, $NO/NO_2/NO_x$ concentrations were measured with a Thermo (Model 42i TL) analyser, and SO_2 concentration was measured with a Thermo (Model 43i TLE) analyser (all Thermo Scientific, Waltham, MA, USA). Stability of all the instruments was excellent (less than 0.16% zero drift over 30 days and less than 0.05% span drift over six months). The lowest level of detection was 0.5 ppb for O_3, < 50 ppt for NO, NO_2 and SO_2. The NO_x analyser uses a molybdenum converter and therefore other oxidised nitrogen compounds like nitric acid (HNO_3) and peroxyacyl nitrates (PAN) are also detected, so the NO_2 concentration denotes actually the sum of all oxidised nitrogen species, NO_y. However, concentrations of these compounds are a small fraction at ppt levels of NO_y.

Calibration of the sensors with standard gases was done in 2013 before the devices were placed at the new SMEAR Estonia site. To avoid transport of the devices to the laboratory in Tartu or to the Estonian Environmental Centre in Tallinn, we did not repeat this procedure yet. The automated calibration system at the SMEAR Estonia station will be available by end of 2015, and a regular automated calibration procedure will be implemented thereafter. On site, the use of a pure air generator (PAG 003, ECO PHYSICS AG, Duernten, Switzerland) was applied monthly to control the zero drift of the sensors.

The wind direction and speed were measured with a Vaisala WXT520 (Vaisala Oyj, Helsinki, Finland) weather transmitter at 2 m above ground, and with a 3D sonic anemometer (METEK uSonic Class A) 30 m above ground, respectively. At the height of 30 m, a shielded and ventilated PT100 temperature sensor (both METEK Meteorologische Messtechnik GmbH, Elmshorn, Germany) was connected.

Data handling

Data from the gas analysers were logged continuously by a computer with a time step of 10 s. Weather data from the weather sensor were transmitted as 10-min averages to the computer system and sonic anemometer and temperature data were logged with 10 Hz on a Raspberry Pi computer (Raspberry Pi® Model B+, Raspberry Pi Foundation, UK) operating with a custom made software. Data were transferred weekly to a storage server.

All the data were examined for corrupted lines of data and underwent spike removal by block averaging in 10-min chunks and calculation of the standard deviation (σ). All values in the interval that exceeded the estimated average by 2.5 times σ were discarded. Most spikes occurred in situations when the devices where switched off for either maintenance, construction activity or when powered back after long power outages. Since the weather transmitter data were already delivered as averaged data, these data were used as provided by the system. In the next step, all the data were transformed into half-an-hourly median values, including quartiles, and stored for further analyses.

The seasonal characterization of ambient trace gas mixing ratios was done by pooling the

data from all the years into monthly chunks and by calculating monthly medians and quartiles.

Using the data on wind statistics obtained from the sonic anemometer operating at the 30-m height, we calculated a density distribution (Fig. 1) representing the probability distribution of wind speed and direction around the measurement site. In order to achieve this, we calculated a probability density function

$$\mathrm{PDF}(\boldsymbol{x}) = \frac{1}{nh}\sum_{i=1}^{n} k\left(\frac{\boldsymbol{x}-\boldsymbol{x}_i}{h}\right), \qquad (1)$$

with a Gaussian smoothing kernel $k(\boldsymbol{x})$, where $\boldsymbol{x}$ denote a random variable of the two dimensional horizontal wind vectors, $\boldsymbol{x}_i$ denote a sample of the wind vector data $\{\boldsymbol{x}_1, \boldsymbol{x}_2, \ldots, \boldsymbol{x}_n\}$ and a bandwidth h which was chosen by Silverman's method (Silverman 1986) assuming a Gaussian distribution on the dataset of length n. The resulting probability density function was then scaled by the wind speed.

In order to classify the possible distant transport of pollution to the site, we further used the wind direction data and defined incoming wind quadrants by north = [315°, 45°), east = [45°, 135°), south = [135°, 225°) and west = [225°, 315°). Pooling the data from the year 2015 into those categories allowed for calculation of median and quartiles of trace gas mixing ratios according to the local incoming wind directions.

In order to distinguish high pollution episodes from background values at the site, we used the median values of the whole data sets, where we added one standard deviation as a cut-off criterion. All the measurements above this threshold where considered transported pollution. Applying the cut-off criterion revealed that 14.9% of the half-an-hour median mixing ratios where above it.

All the data analyses, programming and visualisations were carried out using the Mathematica (Wolfram Research, Inc., Mathematica, version 10.1, Champaign, IL) computing suite.

Air mass trajectory analysis

In order to gain a better insight into the possible source areas of long-range-transported pollution, we used the data obtained from the 30-m measurements since January 2015, as this was the representative time interval during which the measurement system operated continuously without breaks. We picked different occurrences of enhanced SO_2 and NO_x mixing ratios (Table 1) and calculated back trajectories to locate possible distant sources. HYSPLIT (HYbrid Single-Particle Lagrangian Integrated Trajectory; *see* http://www.arl.noaa.gov/HYSPLIT.php) trajectories arriving at 100 m above the ground level were calculated (*see* http://www.ready.noaa.gov). The time interval among trajectories was three hours, and we calculated 48 hours back in time by using NOAA/NCEP GDAS1 archived data (1° horizontal resolution, 2006–present). The results of the model runs were stored and plotted on a map. We added major cities that lie within or near to the trajectory paths as they act as source regions. To calculate the trajectories, we used the web version of the HYSPLIT model (http://ready.arl.noaa.gov/HYSPLIT_traj.php) and for the visualisation Wolfram Mathematica was used.

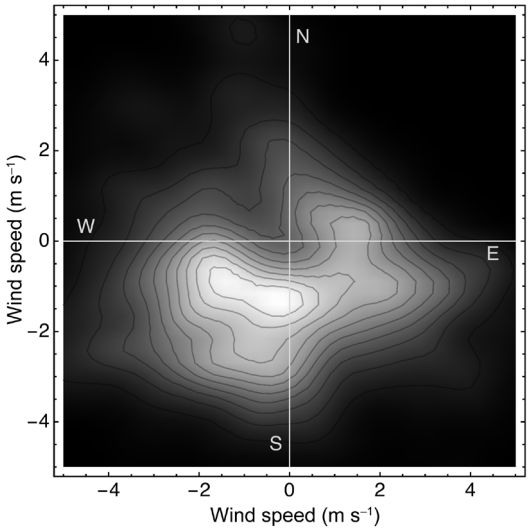

Fig. 1. A representation of the horizontal wind field measured at the 30-m height above ground at the SMEAR Estonia (Järvselja, Estonia). The 130-m mast is located at the origin (0, 0), and the grey scale gives the density of wind vectors, where lighter grey is linked to a higher probability, and therefore higher frequency, of wind vectors occurring at that speed and direction.

Data quality control

The measurements covered the period from

August 2013 until May 2015, accounting for 662 days and leading to a theoretical number of 31 776 half-hour data files to be processed. O_3 measurements were the most robust and, with 29 603 recorded data files, had the lowest number of missing files as compared with the complete number of half-hour files for the measured period. The SO_2 and NO_x analysers had up to 20% losses of recorded data files because they had longer maintenance cycles, and because in autumn 2014 there was an episode where the data transmission to the logging device was interrupted. The number of stored files was 25 628 for SO_2 and 24 852 for NO and NO_2. Quality control measures (filtering and spike removal) led to the removal of about 3% data for O_3, about 10% for SO_2, 6% for NO, and 16% for NO_2. The difference between NO and NO_2, which were measured using the same device, was mostly due to spike removal. While the quality control measures did not change the fraction of removed data for O_3, the quality for SO_2, NO and NO_2 improved.

Results and discussions

Seasonal variation in mixing ratios

The monthly-median ozone mixing ratios showed their maximum in April and their minimum in November (Fig. 2A). This agrees with the results by Eerme *et al*. (2001) who measured total ozone columns over Estonia and found maximum values in March–April and minimum values in October–November. At the SMEAR II station in Hyytiälä (Lyubovtseva *et al*. 2005), the maximum ozone mixing ratios occurred also in April, but the minimum values were observed in September and October and therefore slightly earlier than at the SMEAR Estonia site. The mixing ratios ranged between 5 and 60 ppb in spring, between 0 and 50 ppb in summer and between 0 and 40 ppb in autumn and winter. This covers the same range as reported by Keronen *et al*. (2003) for Hyytiälä. The greater variability in the data from June to September occurred because in that period the pooled data consisted mostly of measurements that were conducted at the 2-m height. As ozone is typically deposited from the atmosphere (Foken *et al*. 2012), it is more likely that the near-surface ozone mixing ratio has higher diurnal variability.

The monthly-median SO_2 mixing ratios ranged between 0.05 to 0.1 ppb during most of the year, with higher values during winter (Fig. 2B). However, there were high values between about 0.2 and 0.4 ppb during July–October. This differs from the seasonal pattern observed in Finland (Riuttanen *et al*. 2013) and Siberia (Lyubovtseva *et al*. 2010). Due to construction activities at the station during July–October, the number of sampled data were sometimes only one third to one fifth of the data obtained during the other months, which led to less accurate mean or median estimation. Given this and the possibility that episodes with high SO_2 concentrations (up to 1.5 to 2 ppb) have greater effects on more limited data sets, the increased median mixing ratios at the SMEAR Estonia site are understandable. Therefore, these monthly medians (*see* grey area in Fig. 2B) are less reliable and can reflect short-term effects of SO_2 sources. One possibility for high SO_2

Table 1. Cases of high and low SO_2 and NO_x mixing ratio episodes measured in 2015. Medians are calculated from the half hour values of the respective month and maximum values are daily maxima. The factor indicates how many times the maximal value exceeds the monthly median mixing ratio. Local wind direction summarizes the wind measured during the daily episode and the trajectory origin where the air mass was located 48 hours before reaching the SMEAR Estonia station.

	Median SO_2 (ppb)	Max. SO_2 (ppb)	Factor	Median NO_x (ppb)	Max. NO_x (ppb)	Factor	Local wind direction	Trajectory origin
28 Feb	0.09	0.7	7.9	1.23	12	9.8	N to SE	NE, S
17 Mar	0.09	2.1	22.8	1.5	11	7.3	SE	E
18 Apr	0.11	1.3	12.04	0.73	1.4	1.9	N	N to W
17 May	0.07	0.09	1.3	0.63	0.9	1.5	W to S	NW

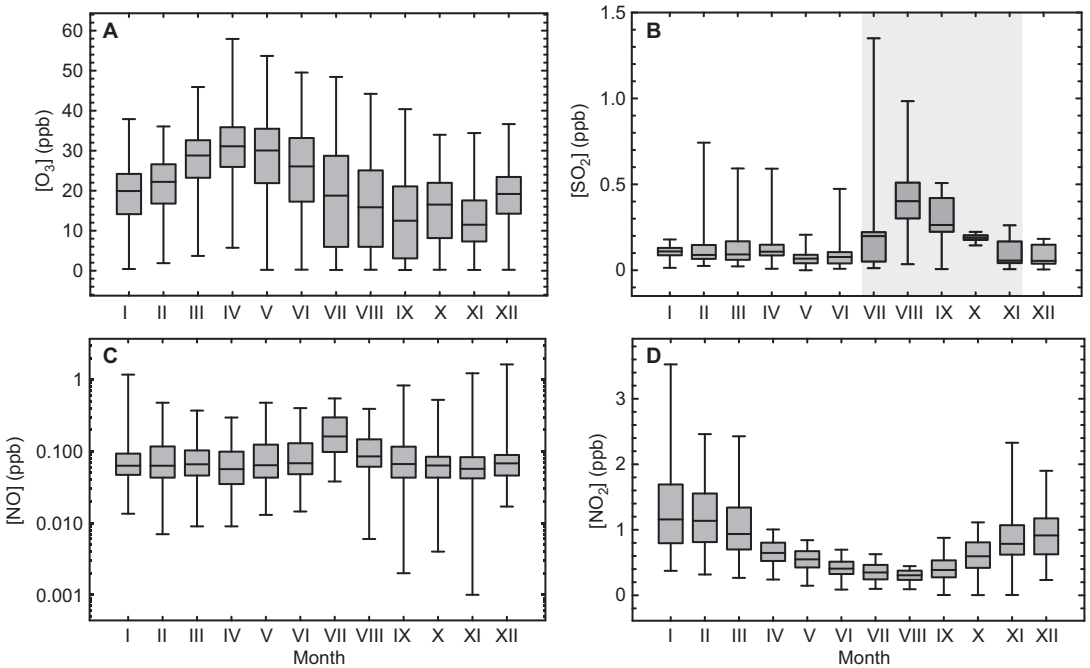

Fig. 2. Monthly mixing ratios of (**A**) ozone, (**B**) sulphur dioxide, **C**) nitric oxide and (**D**) nitrogen dioxide measured at the SMEAR Estonia station in the period between August 2013 and May 2015. Horizontal line in the box shows the median, bottom and top of the box are the 0.25 and 0.75 quartiles, respectively, and whiskers span the value range. The grey area in **B** shows the data that had substantially fewer samples per month due to measurement gaps in 2013 and 2014. For better readability, the nitric-oxide mixing ratio in **C** is given on a logarithmic scale.

mixing ratios are volcanic eruptions and gas release. Since Estonia is located far from potential volcanic sources in terms of the atmospheric lifetime of SO_2, the most probable source for SO_2 was therefore combustion of fossil fuels.

For most of the months, the monthly-median NO mixing ratios were rather stable between 0.06 and 0.07 ppb (Fig. 2C). These values are in line with measurements carried out in a Spruce forest in Germany (Foken *et al*. 2012), and also reflect remote background mixing ratios as measured in Antarctica (Frey *et al*. 2015). Exceptions were July (0.16 ppb) and August (0.09 ppb) with higher concentrations. Although these measurements accurately reflect the prevailing ambient concentrations, those months had about the half of the data coverage, and therefore the same argument as for SO_2 mixing ratios above may apply. The NO mixing ratio had higher variability in winter, which may be due to the fast cycling between NO_2 and NO (Atkinson 2000, Jacob 2000), reflecting the seasonal pattern of the NO_2 mixing ratio.

The monthly-median mixing ratio of NO_2 showed the expected behaviour and was the highest during the winter months (up to 1.2 ppb) and lowest (0.31 ppb) in August (Fig. 2D). This reflects the assumption that mostly anthropogenic combustion of fossil fuels leads to larger emissions in winter (heating) and lower emissions in summer, which was also reported elsewhere (Kulmala *et al*. 2000b, Lyubovtseva *et al*. 2005, 2010).

In general, the second part of the yearly cycle had fewer data because construction activities at the measurement station led to some periods with data gaps for SO_2 and NO_x. Given the resolution of the analysers for SO_2 and NO, the changes in monthly-median mixing ratios were not substantial.

Mixing ratio variation according to local wind direction

To assess the impact of wind direction on the

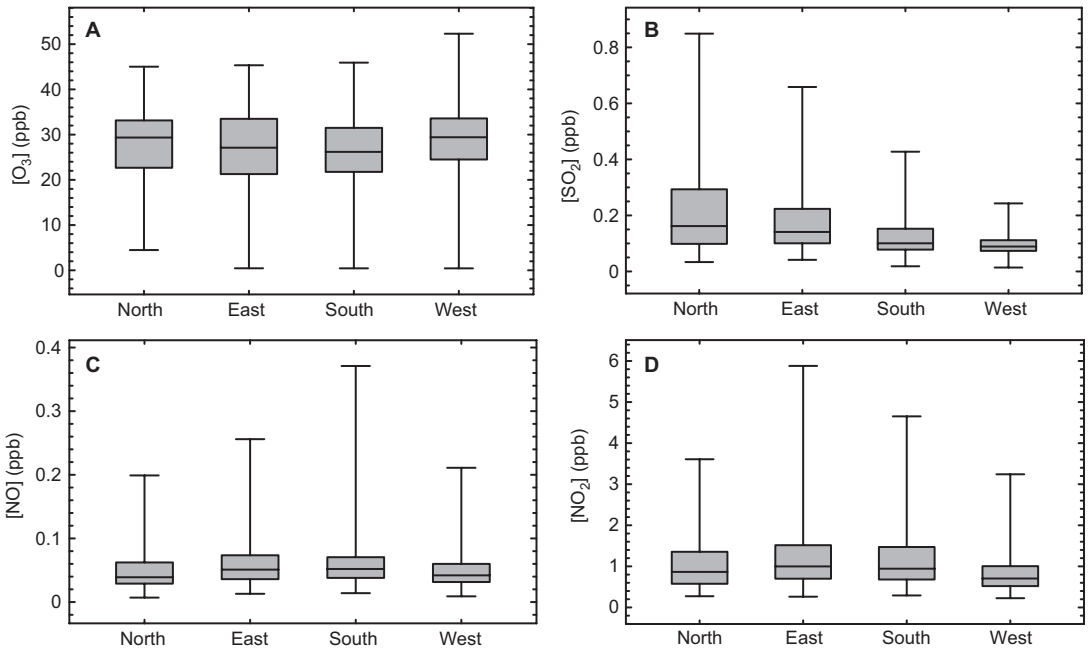

Fig. 3. Mixing ratios categorised by quadrants for (**A**) ozone, (**B**) sulphur dioxide, (**C**) nitric oxide and (**D**) nitrogen dioxide for the period between August 2013 and May 2015. For explanations *see* the caption to Fig. 2.

ambient mixing ratios of O_3, SO_2 and NO_x, we grouped the data into quadrants (Fig. 3). The median mixing ratio of O_3 was similar for north and west (29.4 ppb), while it was the lowest for south (26.2 ppb) and slightly higher for east (27.1 ppb) (Fig. 3A). The largest variations, between 0 to 50 ppb were found for the western wind directions.

The median mixing ratios of SO_2 were the highest in the northern direction (0.16 ppb) and for east (0.14 ppb), south (0.1 ppb) and west (0.09 ppb) the values and variability decreased (Fig. 3B). The maximum values (0.85 ppb) were found in the northern direction. The pattern was different for the NO and NO_2 median mixing ratios (Fig. 3C and D). In case of NO, the highest values of 0.05 ppb were observed for the eastern and southern directions, whereas the lowest value of 0.04 ppb was in the northern direction and a slightly higher value in the western direction (0.42 ppb). For NO_2, the highest value was found for the eastern winds (1 ppb), followed by southern (0.94 ppb), northern (0.87 ppb) and finally western (0.7 ppb) winds.

Those patterns are interesting because the nearest settlement is the Järvselja village about 1.2 km south of the measurement station. Assuming an anthropogenic combustion origin for SO_2 and NO_x, that direction should most likely be related to episodes of high mixing ratios. In case of the short-lived NO, we observed such a relationship, but not for SO_2 and NO_2. The result that SO_2 concentration was the largest for the northern direction was most astonishing, because there are almost no permanently-inhabited settlements in that direction. Also, the wind field density (Fig. 1) supported south and west directions as main origins for high values of the ambient mixing ratios. Using half-hour medians for both wind and gas mixing ratios, we should even out small-scale wind direction changes (Mahrt 2011) originating from small-scale direct effects of the surrounding forest canopy. The surface at the site is flat and there should be no prescribed wind direction because of low terrain elevation.

Taken the above facts together, we conclude that the ambient mixing ratios of SO_2 and NO_2 were mainly affected by distant sources. The high values of SO_2 from northern directions may be explained by the influence of electrical power plants located on the north shore of lake Peipus. The distribution of the ozone mixing

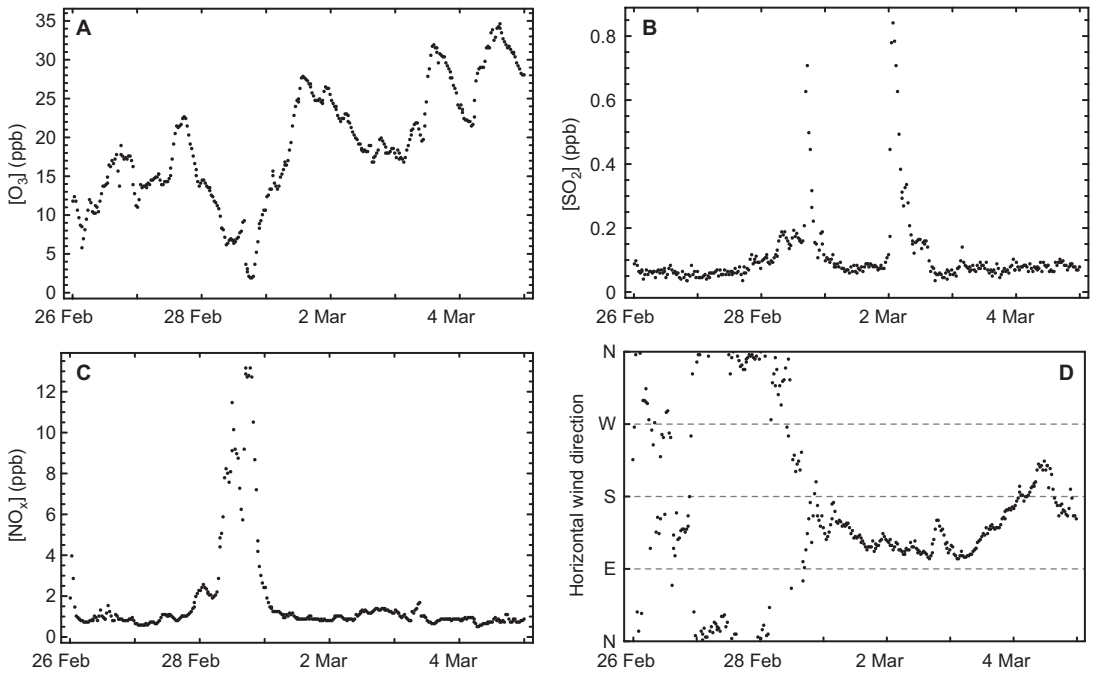

Fig. 4. Median mixing ratios of (**A**) O_3, (**B**) SO_2, (**C**) NO_x and (**D**) horizontal wind direction measured at the 30-m height at SMEAR Estonia during the period between 26 February and 4 March 2015.

ratios according to local wind direction was almost uniform, with a slight preference of west (Fig. 3). Daily variations in ozone mixing ratios were influenced by the diurnal cycle of sunlight and by local sources of VOC released by the forest around the station.

Origin of air masses and trajectory analysis

SO_2 and NO_x have atmospheric lifetimes of about 2–3 days (Lee *et al*. 2011, Riuttanen *et al*. 2013). We used HYPSLIT trajectories to track backwards the origin of air masses over 48 hours. Picking events where either SO_2 or NO_x were higher than their seasonal median mixing ratios led to different scenarios. On 28 February 2015, both SO_2 and NO_x exceeded their monthly median mixing ratios by a factors of 8 and 10, respectively (Table 1, Fig. 4B and C). The O_3 mixing ratio dropped to about 5 ppb (Fig. 4A), which can be due to O_3 titration by the high NO_x and low VOC mixing ratios (Pusede and Cohen 2012) in a situation when the vegetation was still inactive due to winter dormancy (Hakola *et al*. 2009). During the first half of the day, local wind was measured from north, later in the day turning to southeast (Fig. 4D). From the trajectory plot (Fig. 5) the main origin of the air masses was located close to the city of St. Petersburg and later moved to south passing the cities of Riga and Pskov. The high peaks in the SO_2 and NO_x mixing ratios were most probably caused by emissions due to heating in winter and transported to the site.

On 17 March 2015, the SO_2 mixing ratio increased to more than 2 ppb, i.e. by a factor of about 23, and that of NO_x was at 11 ppb, about 7 times higher than the monthly-median value (Table 1, Fig. 6B and C). The trajectories indicated that the air mass originated from the region of Nizhny Novgorod and was passing Moscow. Passing the areas with about 14 million people obviously caused the high load of SO_2 and NO_x in the air arriving at the site, being an example of anthropogenic impact on a background site by distant transport of pollutants. The O_3 mixing ratio dropped to about 20 ppb (Fig. 6A) until the early morning, mostly due to titration by NO_x,

Fig. 5. Trajectories arriving to SMEAR Estonia on 28 February 2015 calculated according to Draxler and Rolph (2013). The red point indicates the location of the SMEAR Estonia station. Map created with Wolfram Mathematica.

but the photochemical O_3 production recovered its mixing ratio until the evening, reaching the value of up to 40 ppb because of rising VOC emissions with increasing vegetation activity at this period of the year. The local wind direction reflected the trajectories origin and travel path (Figs. 6D and 7) with southeast directions.

On 18 April 2015, the SO_2 and NO_x mixing ratios were about 12 and 2 times higher than their monthly-median values, respectively (Table 1, Fig. 8B and C). The trajectories turned from north to west during the day (Fig. 9), passing the industrialised areas in northeast Estonia and the cities of Oslo, Stockholm, Tartu and partly also Tallinn. Ozone followed a typical daily cycle, in which the photochemical ozone production dominates daytime mixing ratios (Fig. 8A). The local measured wind direction was north, turning to west, and did reflect the travel path of the air masses.

On 17 May 2015, low SO_2 and NO_x mixing ratios were observed (Fig. 10). This example may represent typical background mixing ratios at the station when no influence of distant sources occurs. The origin of air masses was the Arctic Ocean northeast of Jan Mayen (Fig. 11). There were no cities in the path of the trajectories except Tartu. Both SO_2 and NO_x mixing ratios were close to their monthly-median values, the daily maximum values exceeding those by the factors of 1.3 and 1.5, respectively (Table 1, Fig.

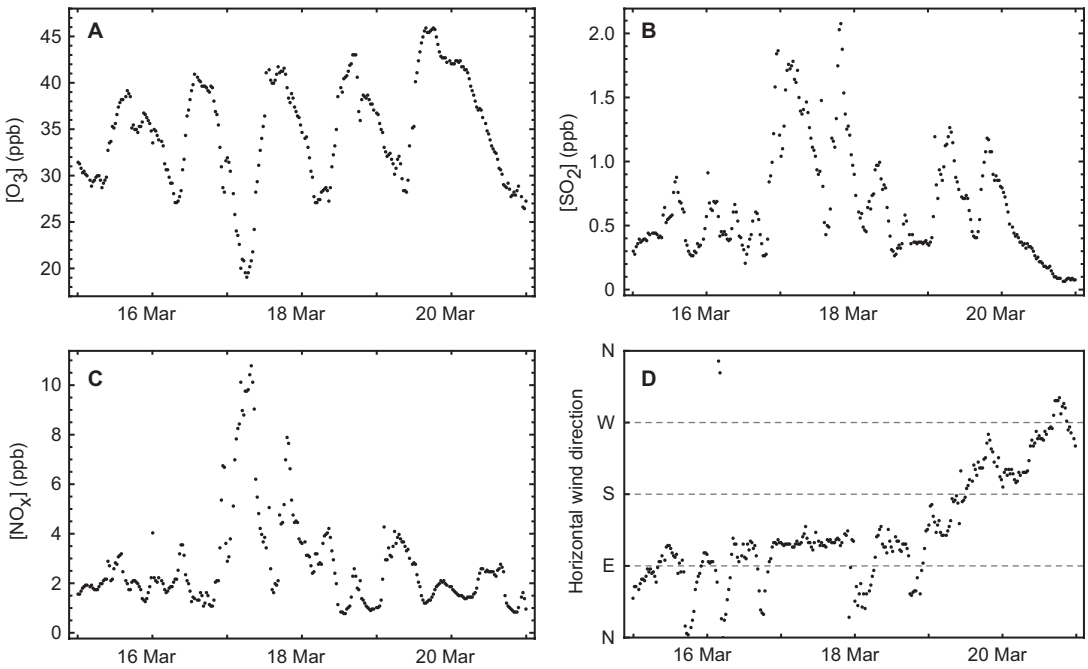

Fig. 6. Median mixing ratios of (**A**) O_3, (**B**) SO_2, (**C**) NO_x and (**D**) horizontal wind direction measured at the 30-m height at SMEAR Estonia for the period 16–20 March 2015.

10B and C). The ozone mixing ratio followed a photochemically-driven daily cycle (Fig. 10A). Therefore, this day was dominated by the local impact of the surrounding forest VOC emissions. Local wind (Fig. 10D) was from west to south during that day and therefore did not reflect the origin of air masses.

A major source of uncertainty in backward trajectory analyses originates from the representation of input data (wind field, meteorological data and vertical transport) that are by themselves uncertain. But also the discretisation procedure that maps the continuous variables onto grid points may lead to temporal and spatial interpolation errors. Estimates of trajectory uncertainty may reach up to 30%–40% of the average distance travelled (Harris *et al*. 2005, Engström and Magnusson 2009).

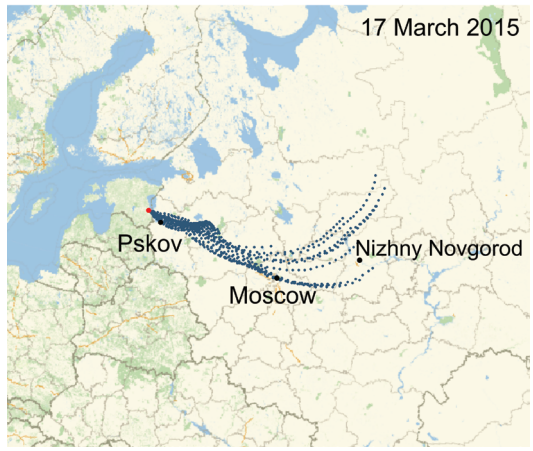

Fig. 7. Trajectories arriving to SMEAR Estonia on 17 March 2015, determined according to Draxler and Rolph (2013). Map created with Wolfram Mathematica.

Discussions and conclusions

Taken together, we can conclude that the hemiboreal SMEAR Estonia site is a clean rural site with weak local pollution sources. The strongest pollution sources are located east and northeast, as was also found at SMEAR II in Hyytiälä, Finland (Kulmala *et al*. 2000b, Riuttanen *et al*. 2013). The most probable sources of SO_2 and NO_x are human activities at distant locations. Local sources, such as soil NO emissions, contribute to background mixing ratios and are

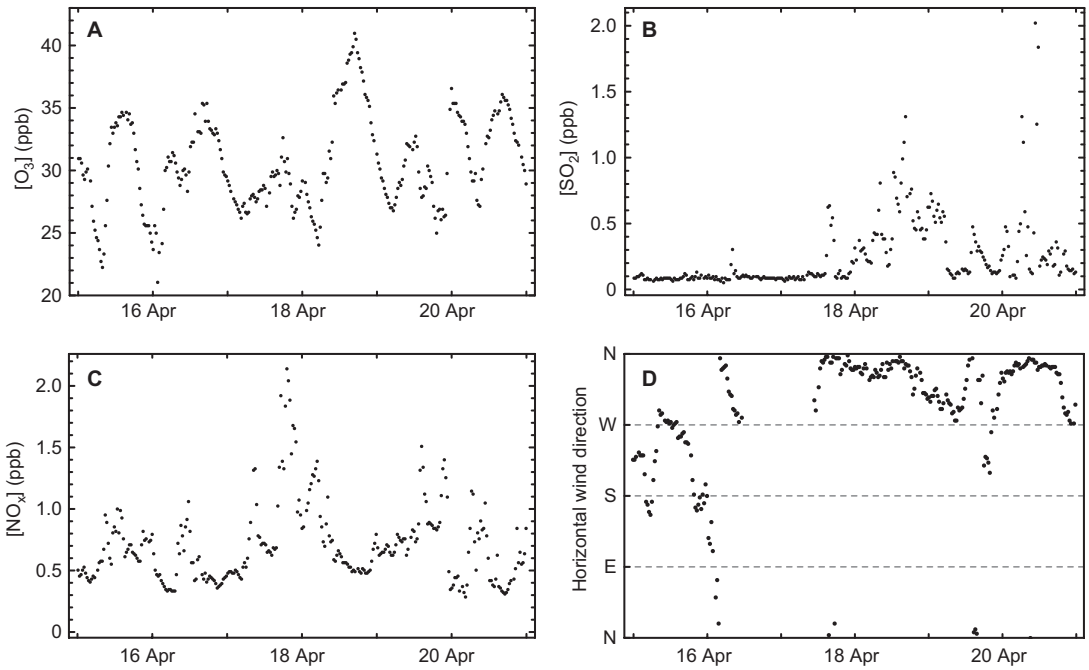

Fig. 8. Median mixing ratios of (**A**) O_3, (**B**) SO_2, (**C**) NO_x and (**D**) horizontal wind direction measured at 30 m height at SMEAR Estonia for the period 16–20 April 2015.

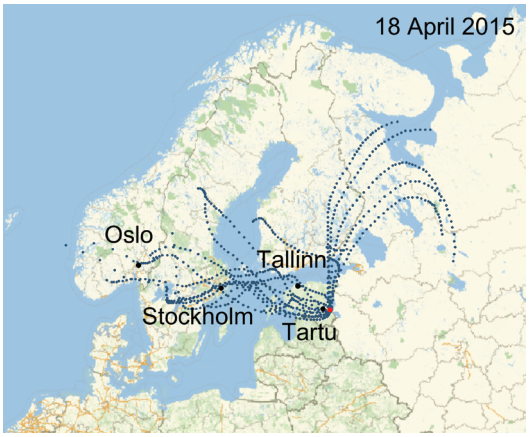

Fig. 9. Trajectories arriving to SMEAR Estonia on 18 April 2015 estimated according to Draxler and Rolph (2013). Map created with Wolfram Mathematica.

typically close to the detection limits of the measurement equipment. The influences of these local sources are overlaid by distant transport (e.g. from NO_2), leading to a concentration pattern over the season where especially NO_2 can be linked to human activities with higher NO_x emissions in autumn and winter. Both local biogenic processes and distant anthropogenic pollutants determined the ozone variability (*see* Figs. 4 and 6), and in that way affect the formation and growth rates of aerosol particles. Since aerosol particles play a role in the formation of clouds and affect the radiative forcing, the interplay of local and distant trace gas sources is an important factor for understanding the climate system.

Prior to 2013, only short periods of measurements were available, so the building of the SMEAR Estonia station enabled the start of continuous measurements with increasing availability and quality of data. The effect of gaps in our data set due to limitations in measurement equipment could clearly be seen in 2014 (Fig. 2B). It also caused a seasonal cycle in the SO_2 mixing ratio that was not very clear. The immediate impacts of local and distant-transported pollution effects on the variability in the data and possible biased medians were visible. Over the whole measurement period, we had 14.9% NO_x and 13.5% of SO_2 mixing ratios associated with distant sources. While relatively infrequent, these events could significantly bias local predictions of ecosystem impacts on air quality and climate.

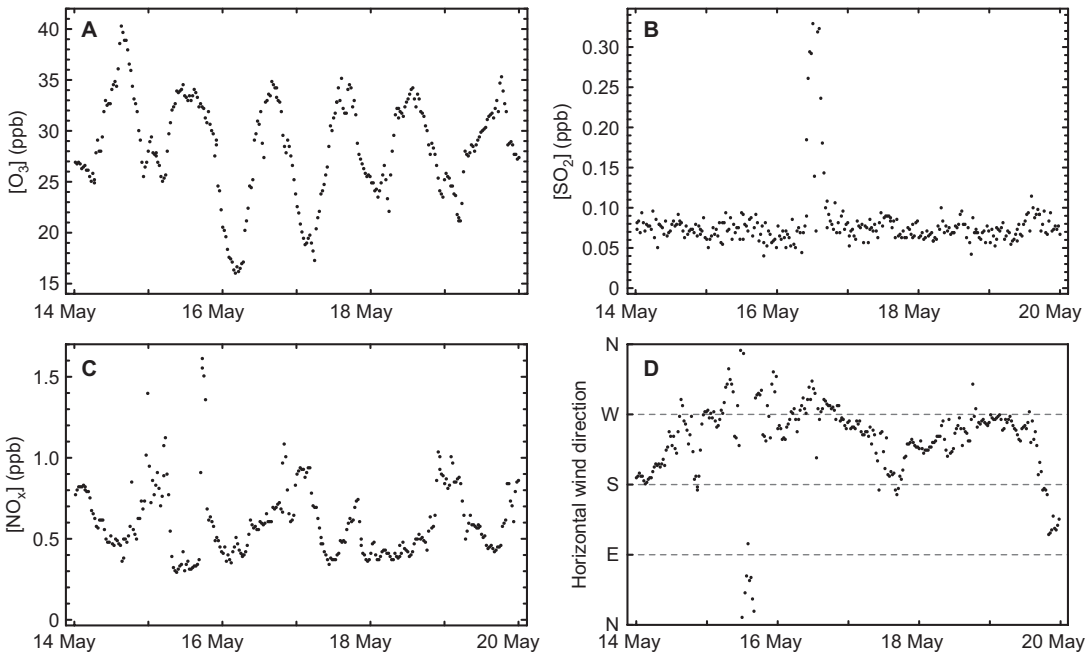

Fig. 10. Median mixing ratios of (**A**) O_3, (**B**) SO_2, (**C**) NO_x and (**D**) horizontal wind direction measured at the 30-m height in SMEAR Estonia for the period 14–20 May 2015.

Fig. 11. Trajectories arriving to SMEAR Estonia on 17 May 2015, simulated according to Draxler and Rolph (2013). Map created with Wolfram Mathematica.

The future development of the SMEAR Estonia station will add more measurement heights and increase the data coverage over the seasons. This should enable comparisons of time series between the Estonian and Finnish measurement sites and elsewhere.

Acknowledgments: The authors received financial support from the European Commission through European Regional Fund [the Centre of Excellence in Environmental Adaptation, the Environmental Conservation and Environmental Technology R&D Programme project BioAtmos (3.2.0802.11-0043), the Internationalization of Science Programme project INSMEARIN (10.1-6/13/1028), the Estonian Research Infrastructures Roadmap project Estonian Environmental Observatory (3.2.0304.11-0395), and the European Research Council (advanced grant 322603, SIP-VOL+)].

References

Atkinson R. 2000. Atmospheric chemistry of VOCs and NO_x. *Atmos. Environ.* 34: 2063–2101.

Bourtsoukidis E., Bonn B. & Noe S.M. 2014. On-line field measurements of BVOC emissions from Norway spruce (Picea abies) at the hemiboreal SMEAR-Estonia site under autumn conditions. *Boreal Env. Res.* 19: 1–15.

Eerme K., Veismann U. & Koppel R. 2001. Estonian total ozone climatology. *Ann. Geophys.* 20: 247–255.

Ehn M., Thornton J.A., Kleist E., Sipila M., Junninen H., Pullinen I., Springer M., Rubach F., Tillmann R., Lee B., Lopez-Hilfiker F., Andres S., Acir I.-H., Rissanen M., Jokinen T., Schobesberger S., Kangasluoma J., Kontkanen J., Nieminen T., Kurten T., Nielsen L.B., Jorgensen S., Kjaergaard H.G., Canagaratna M., Maso M.D., Berndt T., Petaja T., Wahner A., Kerminen V.-M., Kulmala M., Worsnop D.R., Wildt J. & Mentel T.F. 2014. A large source of low-volatility secondary organic aerosol. *Nature* 506: 476–479.

Engström A. & Magnusson L. 2009. Estimating trajectory uncertainties due to flow dependent errors in the atmospheric analysis. *Atmos. Chem. Phys* 9: 8857–8867.

Foken T., Meixner F.X., Falge E., Zetzsch C., Serafimovich A., Bargsten A., Behrendt T., Biermann T., Breuninger C., Dix S., Gerken T., Hunner M., Lehmann-Pape L., Hens K., Jocher G., Kesselmeier J., Lüers J., Mayer J.-C., Moravek A., Plake D., Riederer M., Rütz F., Scheibe M., Siebicke L., Sörgel M., Staudt K., Trebs I., Tsokankunku A., Welling M., Wolff V. & Zhu Z. 2012. Coupling processes and exchange of energy and reactive and non-reactive trace gases at a forest site – results of the EGER experiment. *Atmos. Chem. Phys.* 12: 1923–1950.

Frey M.M., Roscoe H.K., Kukui A., Savarino J., France J.L., King M.D., Legrand M. & Preunkert S. 2015. Atmospheric nitrogen oxides (NO and NO_2) at Dome C, East Antarctica, during the OPALE campaign. *Atmos. Chem. Phys.* 15: 7859–7875.

Hakola H., Hellén H., Tarvainen V., Bäck J., Patokoski J. & Rinne J. 2009. Annual variations of atmospheric VOC concentrations in a boreal forest. *Boreal Env. Res.* 14: 722–730.

Hakola H., Tarvainen V., Laurila T., Hiltunen V., Hellén H. & Keronen P. 2003. Seasonal variation of VOC concentrations above a boreal coniferous forest. *Atmos. Environ.* 37: 1623–1634.

Hari P. & Kulmala M. 2005. Station for Measuring Ecosystem–Atmosphere Relations (SMEAR II). *Boreal Env. Res.* 10: 315–322.

Harris J.M., Draxler R.R. & Oltmans S.J. 2005. Trajectory model sensitivity to differences in input data and vertical transport method. *J. Geophys. Res.* 110, D14109, doi:10.1029/2004JD005750.

Hewitt C.N., Ashworth K., Boynard A., Guenther A., Langford B., MacKenzie A.R., Misztal P.K., Nemitz E., Owen S.M., Possell M., Pugh T.A.M., Ryan A.C. & Wild O. 2011. Ground-level ozone influenced by circadian control of isoprene emissions. *Nat. Geosci.* 4: 671–674.

Hickler T., Vohland K., Feehan J., Miller P.A., Smith B., Costa L., Giesecke T., Fronzek S., Carter T.R., Cramer W., Kühn I. & Sykes M.T. 2012. Projecting the future distribution of European potential natural vegetation zones with a generalized, tree species-based dynamic vegetation model. *Glob. Ecol. Biogeogr.* 21: 50–63.

Holopainen J.K. 2011. Can forest trees compensate for stress-generated growth losses by induced production of volatile compounds? *Tree Physiol.* 31: 1356–1377.

Jacob D.J. 2000. *Introduction to atmospheric chemistry*. Princeton University Press, Princeton.

Jokinen T., Berndt T., Makkonen R., Kerminen V.-M., Junninen H., Paasonen P., Stratmann F., Herrmann H., Guenther A.B., Worsnop D.R., Kulmala M., Ehn M. & Sipilä M. 2015. Production of extremely low volatile organic compounds from biogenic emissions: Measured yields and atmospheric implications. *Proc. Natl. Acad. Sci. USA* 112: 7123–7128.

Karl T., Harley P., Emmons L., Thornton B., Guenther A.,

Basu C., Turnipseed A. & Jardine K. 2010. Efficient atmospheric cleansing of oxidized organic trace gases by vegetation. *Science* 330: 816–819.

Kerminen V.-M., Paramonov M., Anttila T., Riipinen I., Fountoukis C., Korhonen H., Asmi E., Laakso L., Lihavainen H., Swietlicki E., Svenningsson B., Asmi A., Pandis S.N., Kulmala M. & Petäjä T. 2012. Cloud condensation nuclei production associated with atmospheric nucleation: a synthesis based on existing literature and new results. *Atmos. Chem. Phys.* 12: 12037–12059.

Keronen P., Reissell A., Rannik Ü., Pohja T., Siivola E., Hiltunen V., Hari P., Kulmala M. & Vesala T. 2003. Ozone flux measurements over a Scots pine forest using eddy covariance method: performance evaluation and comparison with flux-profile method. *Boreal Env. Res.* 8: 425–443.

Kulmala M. 2004. Organic aerosol formation via sulphate cluster activation. *J. Geophys. Res.* 109, D04205, doi:10.1029/2003JD003961.

Kulmala M., Kerminen V.-M., Laaksonen A., Riipinen I., Sipilä M., Ruuskanen T.M., Sogacheva L., Hari P., Bäck J., Lehtinen K.E.J., Viisanen Y., Bilde M., Svenningsson B., Lazaridis M., Tørseth K., Tunved P., Nilsson E.D., Pryor S., Sørensen L.-L., Hõrrak U., Winkler P.M., Swietlicki E., Riekkola M.-L., Krejci R., Hoyle C., Hov Ø., Myhre G. & Hansson H.-C. 2008. Overview of the biosphere–aerosol–cloud–climate interactions (BACCI) studies. *Tellus* 60B: 300–317.

Kulmala M., Kontkanen J., Junninen H., Lehtipalo K., Manninen H.E., Nieminen T., Petäjä T., Sipilä M., Schobesberger S., Rantala P., Franchin A., Jokinen T., Järvinen E., Äijälä M., Kangasluoma J., Hakala J., Aalto P.P., Paasonen P., Mikkilä J., Vanhanen J., Aalto J., Hakola H., Makkonen U., Ruuskanen T., Mauldin R.L., Duplissy J., Vehkamäki H., Bäck J., Kortelainen A., Riipinen I., Kurtén T., Johnston M.V, Smith J.N., Ehn M., Mentel T.F., Lehtinen K.E.J., Laaksonen A., Kerminen V.-M. & Worsnop D.R. 2013. Direct observations of atmospheric aerosol nucleation. *Science* 339: 943–946.

Kulmala M., Pirjola L. & Mäkelä J.M. 2000a. Stable sulphate clusters as a source of new atmospheric particles. *Nature* 404: 66–69.

Kulmala M., Rannik Ü., Pirjola L., Dal Maso M., Karimäki J., Asmi A., Jäppinen A., Karhu V., Korhonen H., Malvikko S.-P., Puustinen A., Raittila J., Romakkaniemi S., Suni T., Yli-Koivisto S., Paatero J., Hari P. & Vesala T. 2000b. Characterization of atmospheric trace gas and aerosol concentrations at forest sites in southern and northern Finland using back trajectories. *Boreal Env. Res.* 5: 315–336.

Lee C., Martin R.V., Donkelaar A. van, Lee H., Dickerson R.R., Hains J.C., Krotkov N., Richter A., Vinnikov K. & Schwab J.J. 2011. SO_2 emissions and lifetimes: Estimates from inverse modeling using in situ and global, space-based (SCIAMACHY and OMI) observations. *J. Geophys. Res.* 116, D06304, doi:10.1029/2010JD014758.

Lyubovtseva Y.S., Sogacheva L., Dal Maso M., Bonn B., Keronen P. & Kulmala M. 2005. Seasonal variations of trace gases, meteorological parameters, and formation of aerosols in boreal forests. *Boreal Env. Res.* 10: 493–510.

Lyubovtseva Y.S., Zagaynov V.A., Khodzher T.V., Kulmala M., Boy M., Dal Maso M., Junninen H., Obolkin V.A., Potyomkin V.L., Biryukov Y.G. & Lushnikov A.A. 2010. Comparison of formation conditions of secondary aerosol particles in boreal forests of southern Finland and Siberia. *Russ. J. Earth. Sci.* 11: 1–11.

Mahrt L. 2011. Surface wind direction variability. *J. Appl. Meteorol. Climatol.* 50: 144–152.

Noe S.M., Hüve K., Niinemets Ü. & Copolovici L. 2012. Seasonal variation in vertical volatile compounds air concentrations within a remote hemiboreal mixed forest. *Atmos. Chem. Phys.* 12: 3909–3926.

Noe S.M., Kimmel V., Hüve K., Copolovici L., Portillo-Estrada M., Püttsepp Ü., Jõgiste K., Niinemets Ü., Hörtnagl L. & Wohlfahrt G. 2011. Ecosystem-scale biosphere–atmosphere interactions of a hemiboreal mixed forest stand at Järvselja, Estonia. *For. Ecol. Manage.* 262: 71–81.

Pusede S.E. & Cohen R.C. 2012. On the observed response of ozone to NO_x and VOC reactivity reductions in San Joaquin Valley California 1995–present. *Atmos. Chem. Phys.* 12: 8323–8339.

Riuttanen L., Hulkkonen M., Dal Maso M., Junninen H. & Kulmala M. 2013. Trajectory analysis of atmospheric transport of fine particles, SO_2, NO_x and O_3 to the SMEAR II station in Finland in 1996–2008. *Atmos. Chem. Phys.* 13: 2153–2164.

Rollins A.W., Browne E.C., Min K.-E., Pusede S.E., Wooldridge P.J., Gentner D.R., Goldstein A.H., Liu S., Day D.A., Russell L.M. & Cohen R.C. 2012. Evidence for NO_x control over nighttime SOA formation. *Science* 337: 1210–1212.

Silverman B.W. 1986. *Density estimation for statistics and data analysis*. Chapman and Hall, London.

Spracklen D.V, Bonn B. & Carslaw K.S. 2008. Boreal forests, aerosols and the impacts on clouds and climate. *Phil. Trans. R. Soc. A* 366: 4613–4626.

Tunved P., Hansson H.-C., Kerminen V.-M., Ström J., Maso M.D., Lihavainen H., Viisanen Y., Aalto P.P., Komppula M. & Kulmala M. 2006. High natural aerosol loading over boreal forests. *Science* 312: 261–263.

Westervelt D.M., Pierce J.R. & Adams P.J. 2014. Analysis of feedbacks between nucleation rate, survival probability and cloud condensation nuclei formation. *Atmos. Chem. Phys.* 14: 5577–5597.